Pergamon

Int. J. Heat Mass Transfer. Vol. 37, No. 11, pp. 1605–1617, 1994

0017-9310/94 $7.00+0.00

0017-9310(93)0104-O

Natural convection in a hemispherical enclosure heated from below

YASUAKI SHIINA, KAORU FUJIMURA, TOMOAKI KUNUGI and NORIO AKINO

Japan Atomic Energy Research Institute, Tokai-mura, Naka-gun, Ibaraki-ken, 319-11 Japan

(*Received* 21 *July* 1993 *and in final form* 8 *December* 1993)

Abstract—Natural convection in a hemisphere heated from below was studied experimentally. Correlation between heat transfer rate and Rayleigh number was obtained on a hemispherical surface over wide parameter ranges: $10^6 \leqslant Ra \leqslant 6 \times 10^{10}$ and $6 \leqslant Pr \leqslant 13000$. The exponent of Nu against Ra changes from 1/4 to 1/3 at about $Ra \sim 10^9$. Flow patterns in a hemisphere were observed for $2 \times 10^5 \leqslant Ra \leqslant 2 \times 10^9$ and $6 \leqslant Pr \leqslant 13000$. The patterns were classified into several flow regimes, i.e. steady circulating flow, flow with periodic thermal plumes, flow with irregular thermal plumes and turbulent flow regime. Experimental results show that fully turbulent flow regime occurs at $Ra \sim 10^9$.

1. INTRODUCTION

NATURAL convections in enclosures of simple geometries such as rectangle, circle and concentric circle, etc., have been investigated for many years [1–13] in order to understand heat transfer characteristics and the mechanism of onset of convection.

Those investigations do not help us to predict natural convections in enclosures of more complex geometries related with the development of industrial applications such as building systems with complex geometrical spaces and energy systems including nuclear reactors. This would be the reason for the fact that studies on natural convection in enclosures of more complex geometries have increased recently [14–16].

Among many complex geometries, we concentrate on hemispheres. Natural convection in this geometry will be important in the case of loss-of-forced-cooling accident in a pressure vessel of a High Temperature Gas Cooled Reactor. When loss-of-forced-cooling accident occurs, high temperature coolant gas heated by the upper part of the reactor core is transported by natural convection to the upper pressure vessel whose geometry is similar to a hemisphere. Heat transfer and flow characteristics of the natural convection in the pressure vessel must therefore be estimated for the safety analysis of the reactor.

Natural convection in a hemisphere heated from the bottom surface and cooled at the hemispherical surface may have both features of natural convection in a horizontal enclosure and a vertical one. Hereafter, we denote an enclosure as horizontal if the bottom horizontal surface is heated and the top horizontal surface is cooled. We also denote an enclosure as vertical if one of the side vertical walls is heated and the other is cooled. The bottom surface and top region of a hemisphere could locally be regarded as horizontal parallel surfaces and the side region of the hemisphere could be regarded as a vertical surface.

In the case of natural convection in a horizontal enclosure, a conduction state with no flow exists for low Rayleigh number. Steady Bénard convection occurs at the critical Rayleigh number Ra_c, which is independent of Prandtl number but depends on the aspect ratio: $Ra_c \to 1708$ for $L/H \to \infty$ and $W/H \to \infty$, while $Ra_c \to 7000$ for $L/H = W/H \to 1$ [17]. The steady convection roll changes into steady or time-dependent three-dimensional convection patterns with further increase in Rayleigh number [18]. Nusselt number increases from unity as Bénard convection occurs. The exponent of Nusselt number against Ra increases with Rayleigh number because the convection pattern changes. Finally flow becomes fully developed turbulent and Nusselt number changes as $Nu \sim Ra^{1/3}$. For $Pr = 7$, turbulent convection occurs at $Ra \approx 10^5$ [2].

In the case of natural convection in a vertical enclosure, a primary flow due to buoyancy always exists even for weak heating. For large aspect ratios (L/H) with small vertical temperature stratification, unicellular flow is formed below critical Grashof number for $Pr \leqslant 12.45$. Multicellular convection sets in at the critical Grashof number. For $Pr \geqslant 12.45$, on the other hand, a traveling wave sets in at a critical Rayleigh number. For small aspect ratios or strong temperature stratification irrespective of the value of Pr, traveling waves appear [19]. Nusselt number increases from unity when a secondary flow is formed and the departure from conduction regime is retarded for large aspect ratio [20, 21]. For large Rayleigh number with small aspect ratios, Nusselt number changes as $Nu \sim Ra^{1/4}$ [7]. Laminar boundary layer is maintained up to a high Rayleigh number about 10^{10} in the case of aspect ratio of unity [10].

NOMENCLATURE

H	distance between hot and cold surfaces	T_{min}	local minimum fluid temperature
g	gravitational constant	T_+	$T_{max}-T_{av}$
Gr	Grashof number, $g\beta\Delta TR^3/\nu^2$	T_-	$T_{min}-T_{av}$
L	length of enclosure	ΔT	T_h-T_c
Nu	Nusselt number, $Rq/\lambda\Delta T$	W	width of enclosure
$\overline{Nu}$	average Nusselt number	x	distance from the edge of hot surface, $R-r$
Pr	Prandtl number, ν/κ	z	vertical distance from hot surface
q	heat flux	z_h	vertical distance between hot and cold surfaces ($z_h \equiv z_h(r)$)
r	radial distance from the vertical (z) axis (in cylindrical coordinates)	z_{max}	maximum vertical distance where hot thermal plume can reach.
R	radius of hemisphere		
Ra	Rayleigh number based on R, $g\beta\Delta TR^3/\nu\kappa$	Greek symbols	
Ra_x	Rayleigh number based on x, $g\beta\Delta Tx^3/\nu\kappa$	β	coefficient of volumetric thermal expansion
T	temperature	δ	equivalent heat conduction thickness, $R/2\overline{Nu}$
T_{av}	local average fluid temperature	κ	thermal diffusivity
T_b	bulk temperature	λ	thermal conductivity
T_c	temperature of cold surface	ν	kinematic viscosity.
T_h	temperature of hot surface		
T_{max}	local maximum fluid temperature		

To the authors' knowledge, there has been no previous investigation on natural convection in a hemisphere. We do not know whether heat transfer rate by natural convection, flow patterns and transition from laminar to turbulent in a hemisphere are similar to the cases of horizontal enclosures, vertical enclosures or others. Therefore, from the engineering viewpoint, we have to obtain the characteristics of natural convection in a hemisphere to perform safety analysis of High Temperature Gas Cooled Reactor in detail.

The purpose of the present study is to clarify the basic characteristics of natural convection in a hemisphere experimentally with the bottom surface heated and the hemispherical surface cooled. Two kinds of experiment were performed, i.e. heat transfer and flow visualization experiments. Heat transfer rate was measured on a hemispherical surface and flow patterns and temperature fields in the hemisphere were observed. Experimental results were compared with previous data on rectangular enclosures and some results were compared with numerical results.

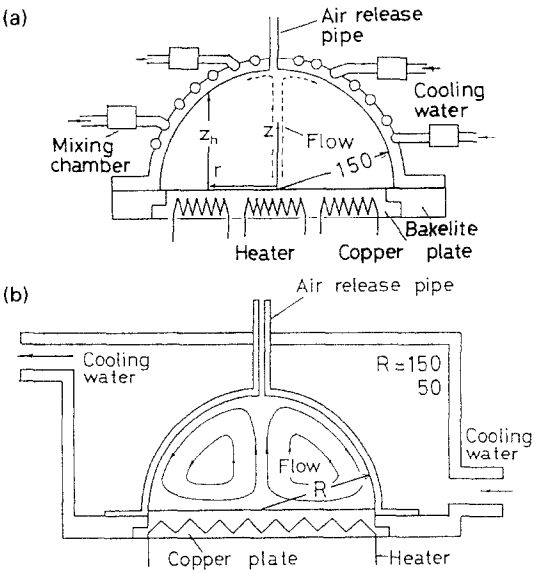

FIG. 1. Schematic diagrams of experimental apparatus. (a) Apparatus for heat transfer experiment. (b) Apparatus for flow visualization experiment.

2. EXPERIMENTAL APPARATUS AND PROCEDURE

Figure 1 shows schematic diagrams of experimental apparatus. Figure 1(a) shows the apparatus for the heat transfer experiment. It consists of a hemispherical shell made of stainless steel 304 (300 mm in inner diameter, 8 mm in thickness) and a heating copper plate (20 mm in thickness). Heat input was supplied with three sheathed heaters soldered in the grooves on the copper plate. The outer surface of the hemisphere was cooled with water flowing through copper tubes soldered on the outer surface. Temperatures of hot and cold surfaces were measured with alumel–chromel thermocouples.

Inner and outer surface temperatures of the hemisphere were measured at fourteen positions located on five concentric regions on the hemispherical surfaces (A–E) as shown in Fig. 2. Four thermocouples were soldered on each position, i.e. two on the inner and two on the outer surfaces. Local heat fluxes were evaluated at each position by solving the heat conduction equation with the use of the measured surface

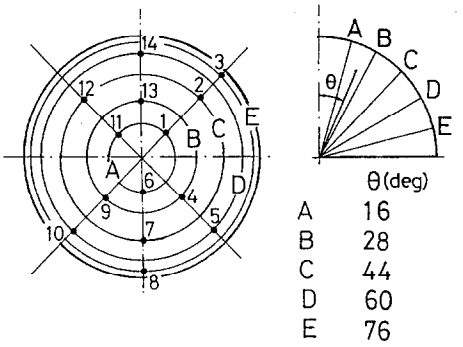

FIG. 2. Positions of thermocouples soldered concentrically on hemispherical surface (regions A–E).

temperatures. Average heat transfer rate on the hemisphere was obtained by the arithmetical average of the calculated local heat fluxes. Errors in estimating the heat fluxes were evaluated to be within $\pm 10.5\%$ including errors in temperature measurement. Heat loss from the hot surface to the atmosphere was measured and evaluated to be in the range of $7 \sim 36\%$ of total heat input.

An air release pipe of 3 mm in inner diameter was welded vertically near the top of the hemisphere at $r = 12.5$ mm as shown in Fig. 1(a). Liquid temperature was measured by I or L-shaped temperature probes with one or two alumel–chromel thermocouples 50 μm in diameter inserted through the air release pipe. The temperature probe was traversed vertically (z-direction). The I-shaped probe has a thermocouple at the end of the straight support pipe and the L-shaped probe has two thermocouples at 14.5 and 75 mm from the end of the support pipe. The latter probe, which was mainly used in the experiment, could measure fluid temperature at two different radial positions simultaneously, whereas it could not measure fluid temperature very near the top of the hemisphere for small radial position.

Water, ethyl alcohol, 78 wt% and 44 wt% aqueous solutions of glycerin, Freon 113 and silicone oils were used as test fluids. Thermal properties of these fluids at 25°C are listed in Table 1. The temperature of the copper plate (hot surface) was kept constant within 0.3°C ranging from 8 to 45°C. The temperature of the cold surface was also kept constant. It scattered dependent on the temperature difference between hot and cold surfaces, ΔT, and the scatter was within 5% of ΔT. Physical properties were estimated at the average temperature between hot and cold surfaces. Ranges of Rayleigh and Prandtl numbers for heat transfer experiment were $10^6 \leqslant Ra \leqslant 5.5 \times 10^{10}$ and $6 \leqslant Pr \leqslant 13\,000$.

Apparatus for the flow visualization experiment is shown in Fig. 1(b). It consists of a transparent outer rectangular enclosure, a hemispherical enclosure made of acrylic resin and a copper plate. The outer surface of the hemisphere was cooled with water flowing between two enclosures. Two hemispheres, 100 and 300 mm in inner diameter and 2 mm in thickness, were made. Thermo-sensitive liquid crystal powder was used as a tracer in order to visualize the flow and temperature fields. Since the color-changing region of the liquid crystal is about $28 \leqslant T \leqslant 32$°C, the hot surface was kept at a temperature of this range in order to distinguish hot fluid by the difference of colors. Vertical and horizontal cross views of natural convection flow were observed by illuminating with a slit light. Non-uniformity in cold surface (hemisphere) temperature was a little larger than the case of heat transfer experiment, within 12% of ΔT. Water, 78 wt% aqueous glycerin and silicone oils were used as test fluids for visualization experiment. Ranges of Rayleigh and Prandtl numbers of the flow visualization experiment were $10^5 \leqslant Ra \leqslant 1.4 \times 10^9$ and $6 \leqslant Pr \leqslant 13\,000$.

3. EXPERIMENTAL RESULTS

3.1. *Heat transfer*

Functional relationship between Nusselt number and Rayleigh number is expressed as

$$Nu = CRa^n Pr^m \tag{1}$$

where C, n and m are empirical constants. Average Nusselt numbers obtained on the hemispherical sur-

Table 1. Specific values of thermal properties of test fluids [30–32].

	ν (10^{-6} m^2 s^{-1})	Pr	β (10^{-4} K^{-1})
Water	0.92	6.3	2.5
78w% aqueous solution of glycerin	31.6	~320	4.4
44w% aqueous solution of glycerin	3.37	~29.4	4.52
Ethyl alcohol	1.39	14.	4.48
Freon 113	0.414	7.9	14.9
Silicone oil KF-96-1000	1000	~9200	9.2
KF-96-100	100	~940	8.9
KF-96-20	20	~195	10

face (cold surface) are plotted against Rayleigh number in Fig. 3.

One of the authors (Y.S.) of the present paper studied laminar natural convection along a hemispherical shell by solving boundary layer equations under an assumption of velocity and temperature profiles which satisfy boundary conditions [22]. Flow velocity and heat transfer rate were obtained by the analysis. The analysis yielded n in equation (1) to be 0.25. In a turbulent region, heat transfer characteristics are expected to depend little on the geometry of enclosures because of high turbulent mixing compared with viscous diffusion near the heat transfer surfaces. This means that a hydraulic length does not appear in heat transfer correlation and therefore the value of n would be equal to 1/3 in the turbulent regime. Since many studies support the expectation, $n = 1/3$ [1, 5, 7], even though slightly lower values of n are also reported [2–4], the value of 1/3 could be adopted as the exponent n in turbulent region for natural convection in a hemisphere. For the value of m, Dropkin and Somerscales [1] postulated as 0.074 and Seki *et al.* [8] as 0.024. Figure 3, however, indicates that the effect of Prandtl number on Nusselt number is not prominent in the present study. With the above consideration, the experimental data can be correlated by the following relationships:

$$\overline{Nu} = 0.185Ra^{0.25} \quad (10^6 < Ra < 10^9) \qquad (2)$$

$$\overline{Nu} = 0.0329Ra^{0.33} \quad (10^9 < Ra < 6 \times 10^{10}). \qquad (3)$$

Equations (2) and (3) indicate that laminar heat transfer would be dominant for $Ra \leqslant 10^9$ and turbulent heat transfer for $Ra \geqslant 10^9$. The above correlations are shown by the solid lines in the figure. The present experimental data are compared with the relationships in horizontal enclosures obtained by Tanaka and Miyata [4] with aspect ratio from 3 to 14 and in vertical enclosures obtained by Bohn *et al.* [10] with aspect ratio to be unity and Seki *et al.* [9] with aspect ratio to be about 4 shown by dotted, broken and chain lines, respectively. Present experimental results lie below the correlations obtained in the horizontal and vertical enclosures. In the cases of horizontal and vertical enclosures, the average heat transfer rates on the hot and cold surfaces are identical

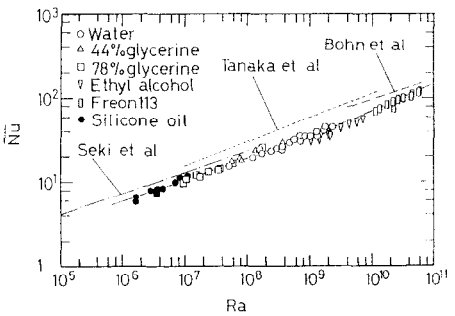

FIG. 3. Plot of average Nusselt number against Rayleigh number.

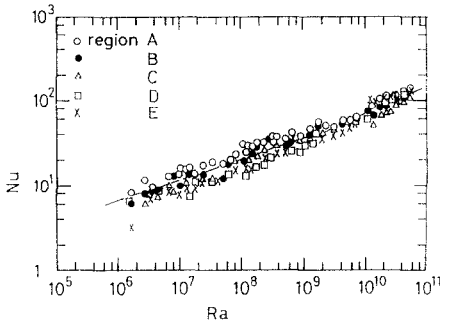

FIG. 4. Plot of local average Nusselt number against Rayleigh number.

because the areas of heat transfer surfaces are the same. For the present case, however, the cold surface is twice as large as the hot surface. Therefore, the average heat transfer rate on the hot surface should be twice that on the cold surface and lies above the correlations obtained in the horizontal and vertical enclosures.

Figure 4 shows the relationship between local average Nusselt numbers and Rayleigh number. Local average Nusselt numbers are obtained by averaging the Nusselt number on each concentric region from A to E shown in Fig. 2. For $Ra < 10^9$, Nusselt number decreases with increasing angle measured from the vertical. For $Ra \geqslant 10^{10}$, however, Nusselt numbers on lower positions (regions D and E) show higher values than on higher positions (region B or region C). We will discuss this point in Section 5.

3.2. *Flow and fluid temperature*

Flow patterns in a hemisphere obtained by the flow visualization experiment are classified into four regimes. The flow regimes are shown against Rayleigh number in Fig. 5. A steady circulating flow is obtained for $Ra < 2 \times 10^5$ (regime 1). Hot thermal plumes are released periodically from the hot surface for $2 \times 10^5 \leqslant Ra \leqslant 4 \times 10^7$ (regime 2). Irregularity is added to regular hot thermal plumes for $4 \times 10^7 < Ra < 10^8$ dependent on Prandtl number and the irregularity becomes dominant for $10^8 < Ra < 10^9$ (regime 3) and flow becomes fully turbulent for $Ra \geqslant 10^9$ (regime 4).

Examples of flow patterns are shown in Fig. 6. The vertical view of the flow and temperature fields for the regime 1 is shown in Fig. 6(a) ($Ra = 1.9 \times 10^5$ and $Pr = 9600$). A steady circulating flow is formed in

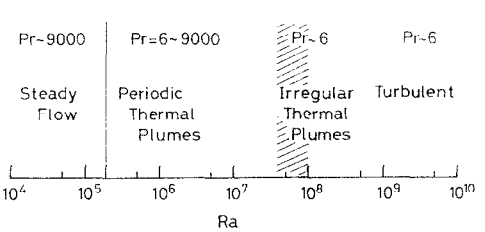

FIG. 5. Plot of flow regimes in a hemisphere against Rayleigh number.

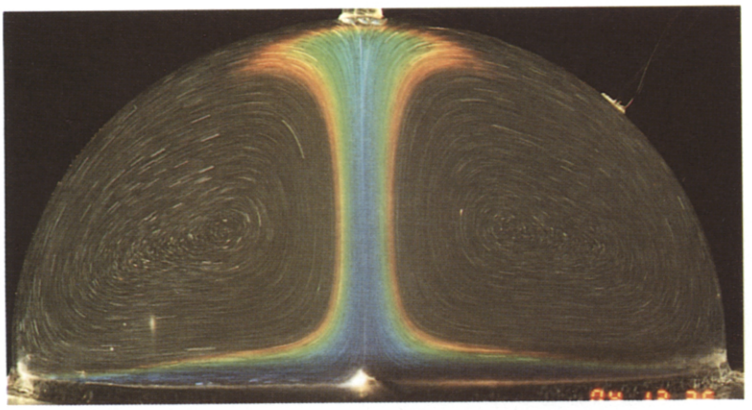

(a) $Ra = 1.9 \times 10^5$, $Pr = 9600$

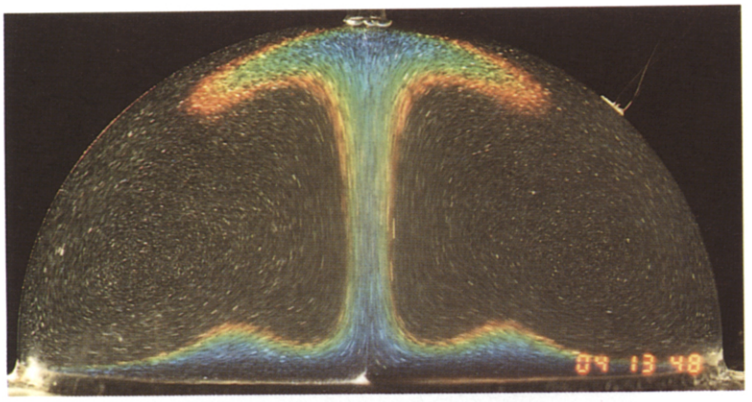

(b) $Ra = 2.3 \times 10^5$, $Pr = 9200$

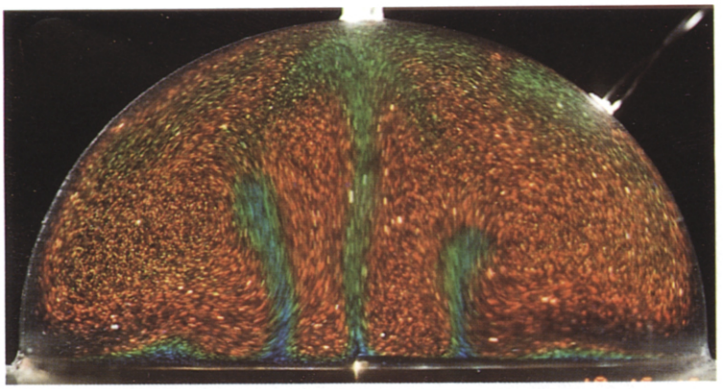

(c) $Ra = 1.6 \times 10^6$, $Pr = 290$

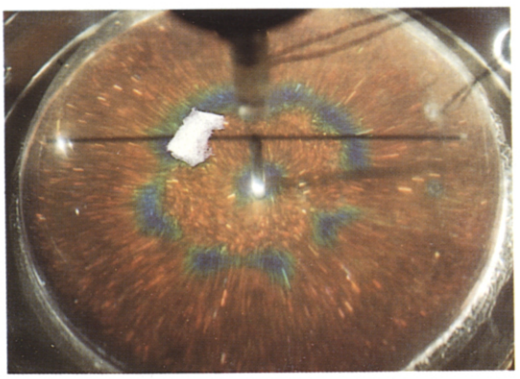

(d) $Ra = 1.6 \times 10^6$, $Pr = 290$

FIG. 6. Flow patterns and temperature fields: (a) $Ra = 1.9 \times 10^5$, $Pr = 9600$; (b) $Ra = 2.3 \times 10^5$, $Pr = 9200$; (c) $Ra = 1.6 \times 10^6$, $Pr = 290$; (d) $Ra = 1.6 \times 10^6$, $Pr = 290$.

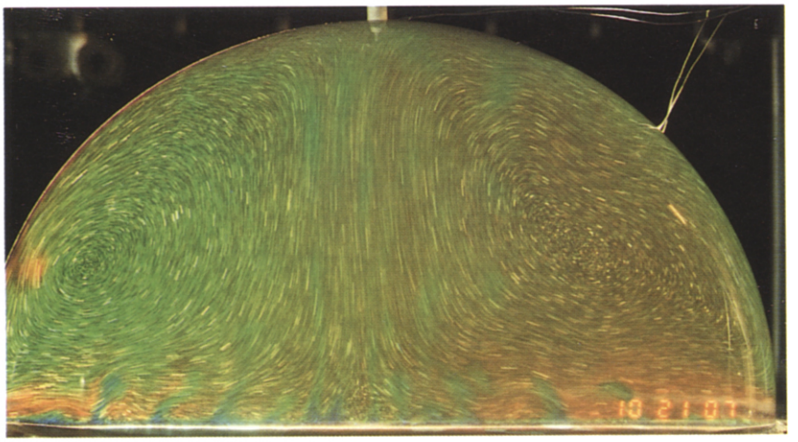

(e) $Ra = 4 \times 10^7$, $Pr = 290$

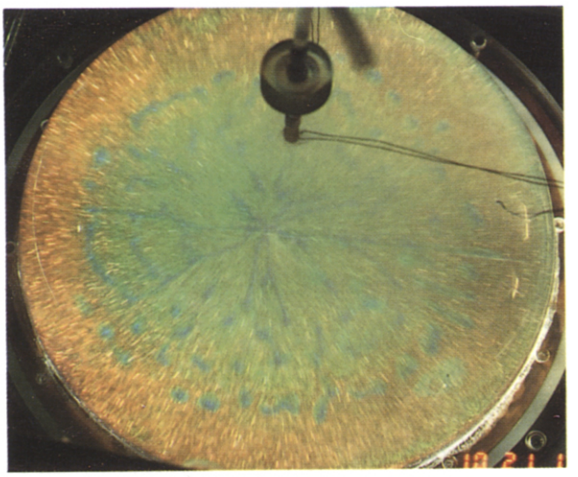

(f) $Ra = 4 \times 10^7$, $Pr = 290$

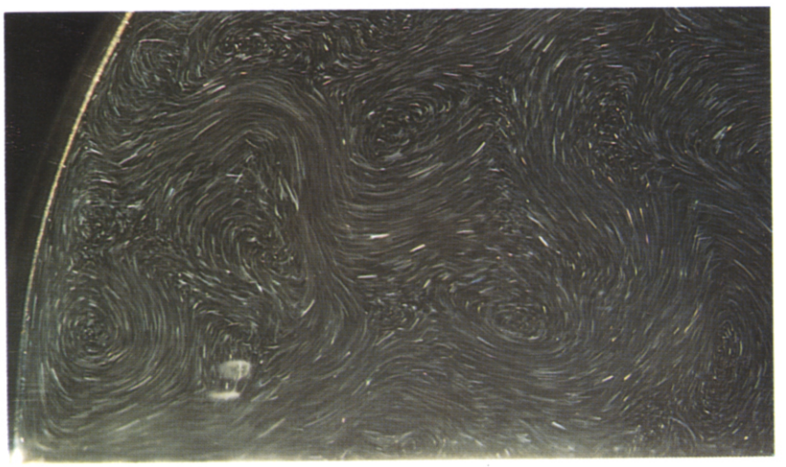

(g) $Ra = 1.4 \times 10^9$, $Pr = 6.5$

FIG. 6.—*continued.* (e) $Ra = 4 \times 10^7$, $Pr = 290$; (f) $Ra = 4 \times 10^7$, $Pr = 290$; (g) $Ra = 1.4 \times 10^9$, $Pr = 6.5$.

the hemisphere. Fluid that flowed towards the center along the hot surface rises upward at the center. After reaching the top of a hemisphere, the fluid flows downward along the hemispherical surface. The thickness of thermal boundary layer increases as flow approaches the center along the hot surface.

With a slight increase in Rayleigh number ($Ra \sim 2\times10^5$ and $Pr = 9200$), a part of the thermal boundary layer swells like a lump at a certain radial position. The lump grows and moves towards the center, then it departs upwards from the hot surface, i.e. the lump is released from the hot surface as a hot thermal plume. Just after this release, the thermal boundary layer becomes very thin, and then it gradually grows and is thickened as time passes. When the thickness is recovered, the next lump is formed at the same radial position and the release process is repeated periodically. A vertical view of the flow and temperature fields is shown in Fig. 6(b). This flow corresponds to an early stage of the periodic thermal plumes (regime 2). Isothermal lines shown by difference in color show a wavy pattern. For a relatively low Rayleigh number in this flow regime, the hot thermal plume is axisymmetric and the release position is located near the center of the hot surface. For a higher Rayleigh number in this regime 2, the axisymmetric structure is broken and three dimensional (discrete) thermal plumes are formed. The release position moves towards the edge of the hot surface. Figures 6(c) and (d) show the other visualized flow patterns and temperature fields ($Ra = 1.6\times10^6$ and $Pr = 290$). For Rayleigh number $Ra \sim 10^6$, a thermal plume is released periodically. Isothermal lines also show a wavy pattern (c). Figure 6(d) is a horizontal view near the hot surface which was taken by using a horizontal slit light. Almost axisymmetric flow could be observed as shown in the figure, although non-axisymmetric structure appeared in the plume. The axisymmetric structure of the hot plumes is broken above $Ra \sim 2\times10^6$. These thermal plumes could be regarded as axisymmetric traveling waves propagating to the center of the hot surface below $Ra \leqslant 2\times10^6$.

Flow patterns and temperature field at $Ra = 4\times10^7$ and $Pr = 290$ are shown in Figs. 6(e) and (f). These flow patterns correspond to a later stage of regime 2. More than two hot thermal plumes could be observed rising up in the figure (Fig. 6(e)). Distribution of the hot thermal plumes on the hot surface was regular. These plumes were released at a fixed radial position close to the edge and flowed towards the center. The amplitude of the wavy structure of isothermal lines near the hot surface is increased towards the center due to rising up of the hot plumes. A horizontal view of hot thermal plumes is shown in Fig. 6(f). The plumes have a three-dimensional structure. Near the edge of the hot surface, discrete plumes are arranged axisymmetrically, whereas near the center, plumes are arranged radially which is similar to the results of Husar and Sparrow [23] on a horizontal hot circular

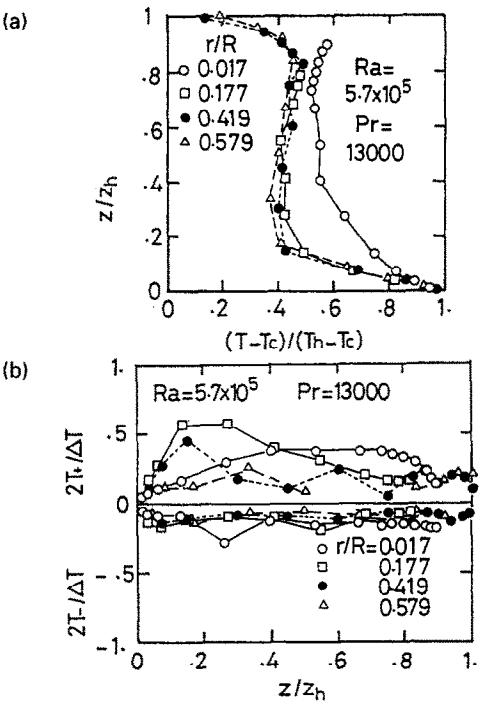

FIG. 7. Results of fluid temperature measurement ($Ra = 5.7\times10^5$, $Pr = 13\,000$). (a) Vertical distribution of average fluid temperature. (b) Vertical distribution of maximum temperature fluctuation.

disc in infinite fluid. We will discuss the behavior of the hot thermal plume in Section 5.

At $Ra = 2\times10^7$ and $Pr = 7$, an irregularity was observed in the flow pattern in the central region of the enclosure in spite of low Rayleigh number compared with Fig. 6(e). This flow corresponds to the early stage of region 3. The appearance of the irregular flow depends on Prandtl number and the boundary between region 2 and region 3 is somewhat obscure (because of this, shadowed hatches are used in Fig. 5). In this case, however, hot thermal plumes were still released regularly from the hot surface.

These irregularities are increased with Rayleigh number for $Ra \geqslant 10^8$ and finally flow becomes turbulent for $Ra > 10^9$ (regime 4). Figure 6(g) shows a flow pattern at $Ra = 1.4\times10^9$ and $Pr = 6.5$. In the figure, irregular eddies are observed in the fluid. Large circulating flow could not be observed explicitly in the experiment.

Results of fluid temperature measurement are shown in Figs. 7–9. In the figures, (a) and (b) show the vertical distribution of the average fluid temperature $(T-T_c)/\Delta T$ and the vertical distribution of the maximum fluid temperature fluctuations $2T_-/\Delta T$ and $2T_+/\Delta T$, respectively. The average fluid temperature was obtained by averaging the base fluid temperature which is obtained by filtering out temperature fluctuations due to hot thermal plumes. The maximum fluid temperature fluctuations T_+ and T_- were obtained by measuring the deviation of maximum or minimum fluid temperatures from the average fluid

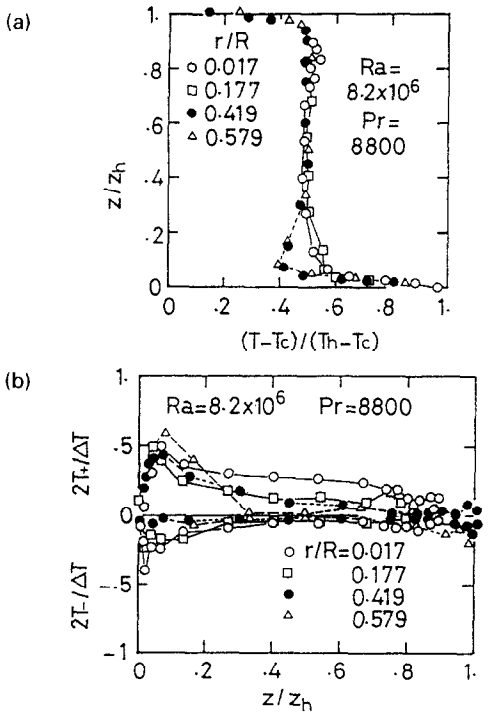

FIG. 8. Results of fluid temperature measurement ($Ra = 8.2-10^6$, $Pr = 8800$). (a) Vertical distribution of average fluid temperature. (b) Vertical distribution of maximum temperature fluctuation.

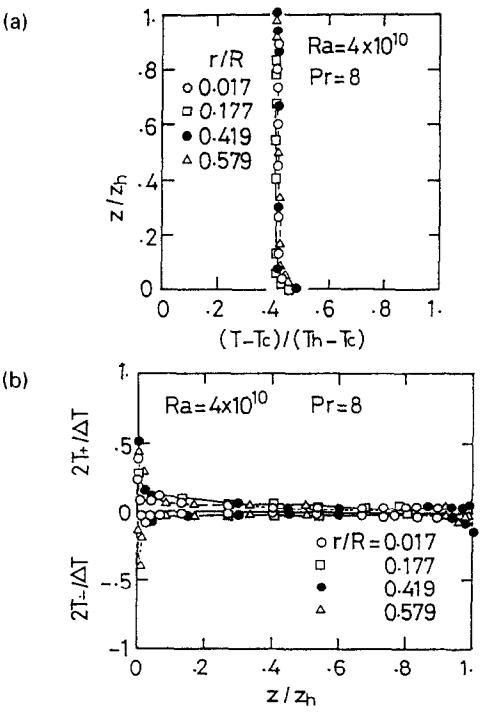

FIG. 9. Results of fluid temperature measurement ($Ra = 4 \times 10^{10}$, $Pr = 8$). (a) Vertical distribution of average fluid temperature. (b) Vertical distribution of maximum temperature fluctuation.

temperature. As is previously described, the fluid temperature near the top of the hemisphere for small radial positions could not be measured by the use of the L-shaped temperature probe.

Figure 7 shows the results of temperature measurement for the early stage of regime 2 at $Ra = 5.7 \times 10^5$ and $Pr = 13000$. Fluid temperature decreases with increase in r/R due to the steady upward flow at the center of the enclosure. Distributions of the average fluid temperature show an inverse-S-shaped profile except for $r/R \sim 0$. This is explained to be due to the flow circulation. Hot fluid which rises up from the hot surface in the center region is cooled during flowing down along the hemispherical surface and the resultant cold fluid flows on the hot surface. As shown in Fig. 7(b), temperature fluctuations are large for all the vertical distance from the hot surface to the top of the hemisphere. Traces of fluid temperature are shown in Fig. 10(a). Periodic fluctuations are seen.

Figure 8 shows the case of $Ra = 8.2 \times 10^6$, $Pr = 8800$ (regime 2). Average fluid temperatures measured at four different radial positions are almost the same except in the vicinity of the hot surface as shown in Fig. 8(a). This type (boundary layer-type) of temperature profile was formed above $Ra \sim 10^6$. Average fluid temperatures near the hot surface at $r/R = 0.419$ and 0.579 are considerably low. Therefore, fluid temperature reversal was observed which was apparently similar to the natural convection in horizontal enclosures [2]. However, the cause of the temperature reversal was different from that of the horizontal enclosure. For the case of horizontal enclosure, the temperature reversal is caused by blobs of stagnant hot or cold fluid near the cold and hot surface, respectively [2]. In the present case, however, the temperature reversal near the hot surface is caused by cold fluid flowed down along the hemispherical surface. Figure 8(b) shows that temperature fluctuation is large for all of z at small r/R. At $r/R \geqslant 0.419$, however, the temperature fluctuations become small for $z/z_h \geqslant 0.4$, which indicates that the hot thermal plumes reach the center before they rise up to the inner surface of the hemisphere. Therefore the plumes do not exist for $r/R \geqslant 0.4$ except near the hot surface. Time traces of the fluid temperature at this stage are shown in Figs. 10(b,c). Periodic fluctuations could be seen near the hot surface. Near cold surface, cold thermal plumes were observed as shown in Fig. 10(c). The number of cold plumes observed in a unit time, however, is considerably smaller than that of hot thermal plumes. Due to continuity, fluid must flow down from the cold surface corresponding with the rising hot thermal plumes. The existence of descending flow along the hemispherical surface reduces the frequency of cold thermal plumes.

Similar characteristics observed in fluid temperature at $Ra = 8.2 \times 10^6$ could be observed up to $Ra \sim 10^8$ (regime 3). At $Ra = 1.6 \times 10^8$ and $Pr = 280$, the maximum temperature fluctuation was high at $r/R \sim 0$ as was similar to the case of $Ra = 8.2 \times 10^6$.

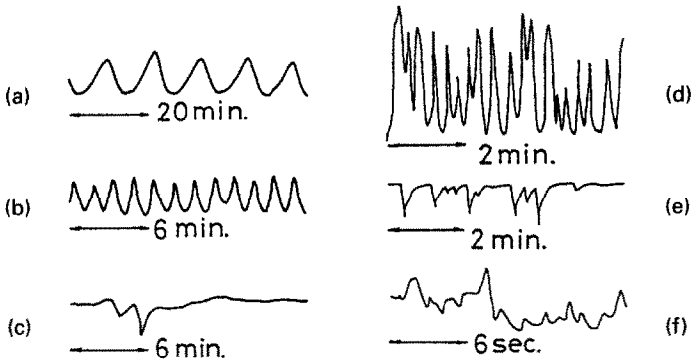

FIG. 10. Time traces of fluid temperature fluctuations: (a) $Ra = 5.5 \times 10^5$, $Pr = 13\,000$, $r/R = 0.419$, $z/z_h = 0.1$; (b) $Ra = 8.2 \times 10^6$, $Pr = 8800$, $r/R = 0.579$, $z/z_h = 0.02$; (c) $Ra = 8.2 \times 10^6$, $Pr = 8800$, $r/R = 0.579$, $z/z_h = 0.88$; (d) $Ra = 1.6 \times 10^8$, $Pr = 280$, $r/R = 0.579$, $z/z_h = 0.02$; (e) $Ra = 1.6 \times 10^8$, $Pr = 280$, $r/R = 0.579$, $z/z_h = 0.92$; (f) $Ra = 4 \times 10^{10}$, $Pr = 8$, $r/R = 0.579$, $z/z_h = 0.01$.

It clearly suggests the existence of circulating flow which rises at the center of the hot surface and descends along the cold surface. Figures 10(d) and (e) show the time traces of fluid temperature near the hot and cold surfaces at this stage, respectively. Irregular fluctuations appeared in the fluid temperature but the fluctuations are rather periodic near the hot surface as shown in Fig. 10(d). The frequency of the cold thermal plume is seen to be increased but still lower than that of the hot one (e).

Figure 9 shows temperature results at $Ra = 4 \times 10^{10}$ and $Pr = 8$ (regime 4). Average fluid temperatures at different radial positions are almost identical to each other. Temperature fluctuations are confined very near the hot and cold surfaces. Temperature fluctuations for $r \sim 0$ are very small as shown in Fig. 9(b). Time traces of fluid temperature fluctuations shown in Fig. 10(f) show no regular motions. These results indicate that there is no dominant circulating flow in the enclosure and thermal hot plumes would be released randomly. The hot plumes would be dissipated in surrounding fluid immediately after the release from hot surface, as is discussed in next subsection.

3.3. *Maximum arrival distance of hot thermal plumes*

Maximum arrival distances of hot thermal plumes at various r/R are shown in Fig. 11. The distance was determined by measuring a distance $z = z_{max}$ at which the temperature fluctuation to higher side due to the plumes disappeared in the time traces of fluid temperature. In the case of $Ra = 5.7 \times 10^5$, the open circles with uparrow at $r/R = 0.017$ and 0.177 mean that the thermal plumes would reach closer to the hemispherical surface because the temperature fluctuations due to the plumes were very large at the positions. In this case, hot thermal plumes reach the inner surface of the hemisphere (i.e. $z/z_h = 1$) even if $r/R = 0.58$ (away from the center region). For $10^6 \leqslant Ra \leqslant 10^8$, as is discussed in the previous subsection, hot thermal plumes at $r/R \sim 0$ reach the inner surface of the hemisphere, however z_{max} decreases rapidly with increase

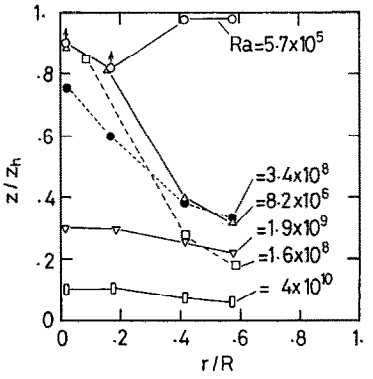

FIG. 11. Plot of maximum arrival distance of hot thermal plumes against r/R.

in r/R. For $Ra > 10^9$, hot thermal plumes cannot reach the inner surface of hemisphere even if $r/R \sim 0$.

Figure 12 shows correlation between the maximum arrival distance of hot thermal plumes z_{max} at $r \sim 0$ against Rayleigh number. The value of z_{max} was normalized by an effective conduction thickness δ on the hot surface defined by

$$\delta = R/2\overline{Nu}. \tag{4}$$

Heat transfer coefficient is virtually determined in the small regions near the surfaces.

In the figure, the solid line corresponds to the top of hemisphere, that is,

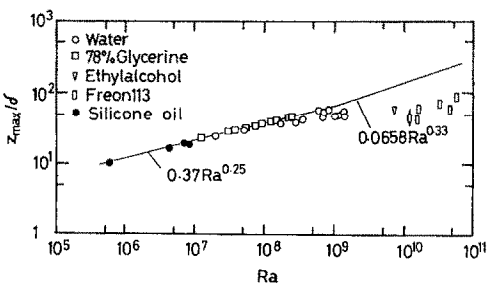

FIG. 12. Plot of maximum arrival distance of hot thermal plumes at $r/R \sim 0$ against Rayleigh number.

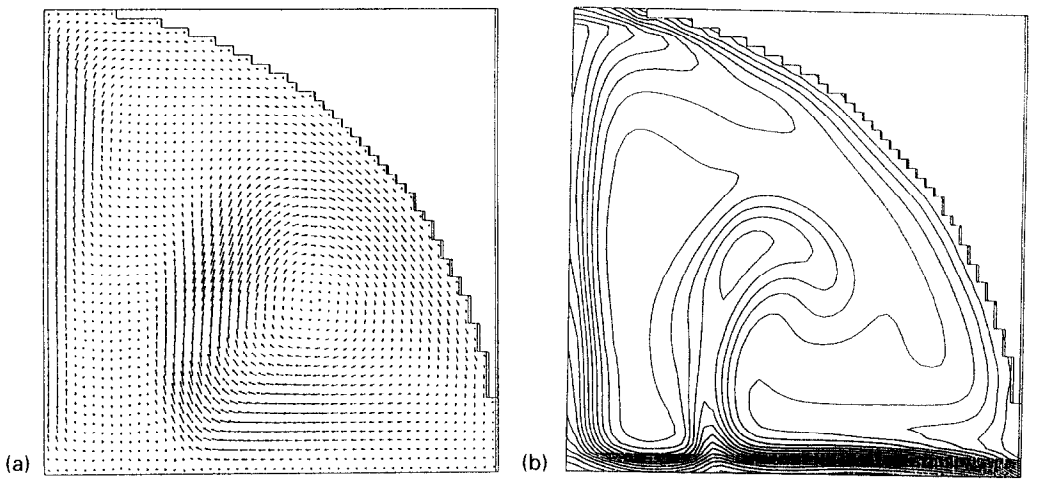

FIG. 13. Numerical results ($Ra = 2 \times 10^6$, $Pr = 850$). (a) Velocity vectors. (b) Isothermal lines.

$$R/\delta = 2\overline{Nu} = 0.37Ra^{0.25} \quad (10^6 < Ra < 10^9) \quad (5)$$

$$R/\delta = 2\overline{Nu} = 0.0658Ra^{0.33} \quad (10^9 < Ra < 5 \times 10^{10}). \quad (6)$$

As shown in the figure, hot thermal plumes arrive at the top of the hemisphere for $Ra < 5 \times 10^8$. For $Ra > 5 \times 10^8$, however, the value of z_{max}/δ lies below the solid line and it takes a constant value of $50 \sim 70$. For $Ra > 5 \times 10^8$, z_{max} decreases with increase in Rayleigh number, i.e. hot thermal plumes do not reach the top of the hemisphere and are dissipated in the surrounding fluid by turbulence dissipation. The value of $z_{max} = 50 \sim 70$ is still larger than $z_{max} \approx 20$ for the case of horizontal enclosures [4]. It indicates that there is still very weak circulating flow and upward flow at the center region raises the thermal plumes

4. COMPARISON WITH NUMERICAL RESULTS

Natural convection in a hemisphere was solved numerically under an assumption of axisymmetry. Boundary configuration of a hemisphere was simulated by accumulated thin circular discs because of the usage of the cylindrical (r,z) coordinate system and corresponding velocity components (u,w). Mesh numbers in (r,z) direction were 50×50. Scalar quantities such as pressure and temperature were defined at the center of the each control volume and velocity was defined at the surface center. We used the well-known semi-implicit method for pressure linked equations (SIMPLE method [24]). Numerical analyses were performed for conditions of $Ra = 10^5$, $Ra = 5 \times 10^5$, 10^6, and $Ra = 2 \times 10^6$ with $Pr = 850$ and $Ra = 3.6 \times 10^6$ with $Pr = 7$. In the analyses, calculations were performed until steady or periodic solutions were attained, i.e. after about 4×10^4 s in real time.

Steady flow was obtained for $Ra \leqslant 10^6$. For $Ra \geqslant 2 \times 10^6$, steady flow could not be obtained and flow with periodic thermal plumes was obtained. In the flow visualization experiment, we obtained $Ra = 2 \times 10^5$ as Rayleigh number for the onset for periodic thermal plumes. This value is much lower than the numerical analysis. Some reasons would be considered for the discrepancy, i.e. non-uniformity in hot and cold surface temperatures in the experiments and some defects in the apparatus such as distortion and non-axisymmetry may cause lower onset Rayleigh number. Effects of non-axisymmetry of the apparatus, however, seems to give insignificant effects on flow because almost axisymmetric flow patterns could be observed in the experiment below $Ra \sim 2 \times 10^6$.

Figure 13 shows velocity vector and isothermal lines at $Ra = 2 \times 10^6$ and $Pr = 850$. Comparison of the analysis with the experimental results (Fig. 6(c)) shows similarity in thermal plumes which are almost axisymmetric in the experiment. Although the onset Rayleigh number is different between analysis and experiment, flow pattern and temperature fields in two flow regimes of steady and periodic thermal plumes would be similar as far as axisymmetry is satisfied.

Average Nusselt number on the hemispherical surface is plotted against Rayleigh number in Fig. 14. The solid line shows equation (2) and the broken line is its extrapolation. The exponent of the numerical results between Nusselt and Rayleigh numbers is nearly equal to 0.2 for $Ra \leqslant 10^6$, which corresponds to boundary layer flow of natural convection on a

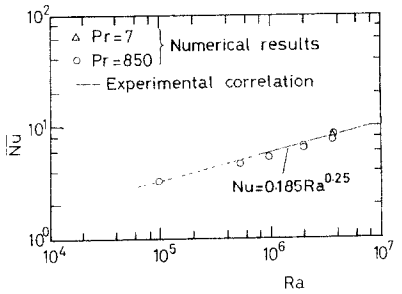

FIG. 14. Heat transfer correlation in numerical results.

heated circular disc [25] and nearly equal to 0.25 for $Ra \geqslant 2 \times 10^6$ which corresponds to boundary layer flow of natural convection along hemispherical shell [22]. This suggests that the dominant heat transfer mechanism is boundary layer flow on the horizontal hot surface for $Ra \leqslant 10^6$ and boundary layer flow along cold hemispherical surface for $Ra \geqslant 2 \times 10^6$. The Nusselt number obtained from the numerical analysis agrees well with the extrapolated line. Three dimensional numerical analysis will be necessary for more precise comparison at higher Rayleigh numbers since axisymmetrical thermal plumes are broken above $Ra \sim 2 \times 10^6$ in the experiment.

5. DISCUSSION

Natural convection in a hemispherical enclosure heated from below would have both characteristics of those in horizontal and vertical enclosures. The aspect ratio of a hemisphere is about unity.

For the case of natural convection in vertical enclosures with aspect ratio to be unity, transition from laminar to turbulent occurs at high Rayleigh number and laminar boundary layer is maintained along vertical surface even at $Ra \sim 10^{10}$ according to Bohn *et al.* [10]. The transition is induced by a traveling wave instability. On the other hand, for horizontal enclosures, the transition occurs at $Ra = 10^4 \sim 10^5$ for water. This Rayleigh number is considerably lower than that in vertical enclosures. The characteristic of turbulent natural convection in horizontal enclosures is random release of hot thermal plumes (which are usually called as thermals in horizontal enclosures) from the hot surface. There is no dominant flow in enclosure in this case.

For the present case, the hot surface and the top region of hemisphere cause a flow similar to a horizontal enclosure, whereas the hemispherical surface except for the top region causes a flow similar to vertical enclosures. For comparatively low Rayleigh number, a laminar boundary layer will be developed along the hemispherical surface and this type of flow dominates heat transfer mechanisms of the inner surface of a hemisphere. Heat transfer rate decreases towards the flow direction. Therefore, the results of local average Nusselt number shown in Fig. 3, where Nusselt number decreased from region A to E in alphabetical order for $Ra \geqslant 10^9$, support the existence of the boundary layer flow along the hemispherical surface. For higher Rayleigh number, randomness in flow induced by hot thermal plumes is considerably increased and flow becomes turbulent before the boundary layer flow along the hemispherical surface turns into turbulent. The results of the experiments, i.e. heat transfer, fluid temperature measurement and flow visualization, indicate that flow becomes fully developed turbulent at $Ra \sim 10^9$. Because of this transition, the boundary layer flow vanishes for Ra 10^9. For this Rayleigh number, regime 4, heat would be transferred by the similar mechanism of turbulent natural convection in horizontal enclosures, i.e. heat is transported mainly by hot and cold thermal plumes which ascend or descend almost vertically. Since the distance between the hot and cold surfaces is changed dependent on r/R, heat transfer rate would be higher in the region of small distance. This would be the cause that the local average Nusselt numbers at region D and E were increased and became higher than region B and C for Ra 10^{10} as shown in Fig. 4. However, the reason why Nusselt number of region A is still higher than regions D and E is not clear.

Natural convection flow would be influenced by Prandtl number. According to Rossby [2], onset Rayleigh number for the irregular flow depends on $Pr^{0.6}$. Seki *et al.* [7] reported that transition from laminar to turbulent occurred at a lower Rayleigh number for water than for glycerin and oil. In the present study, irregular motion was observed in the center region of the enclosure at $Ra \sim 2 \times 10^7$ for $Pr = 7$ and not observed for $Pr = 280$ at $Ra \sim 4 \times 10^7$. In both cases, however, plumes were generated regularly near the hot surface. This suggests that irregular motion is initiated away from the hot surface. Effects of Prandtl number on flow pattern must be investigated in future work.

Let us now discuss the periodic release of hot thermal plumes from the bottom surface. As we have already mentioned in Sub-section 3.2, the periodic release should be understood as a traveling wave which propagates in the r direction toward the center. Indeed, one plume is composed of a pair of counter-rotating vortices, and periodic array of vortices corresponds to waves. The present physical setup involves the circulating primary flow even for very small temperature difference. The flow therefore can be regarded as a basic flow for the unstably stratified fluid above the heated surface. The periodic release is due to an instability of such basic flow field.

A through flow exerts a pattern selection mechanism on a Rayleigh–Bénard convection, i.e. longitudinal stationary roll is the critical mode if the Reynolds number of the through flow is relatively small. Here we denote a roll whose axis aligns in the streamwise direction as a longitudinal roll, which is of course due to a buoyancy driven instability. The critical Rayleigh number is independent of a Reynolds number of the through flow as far as the Reynolds number is below the critical value for the isothermal through flow [26]. Beyond the critical Reynolds number, on the other hand, hydrodynamic instability mode called the Tollmien–Schlichting waves sets in.

Some experimental works concerning the stability for free convection boundary layers on heated inclined plates show that rolls can be the dominant disturbance [27]. Traveling wave disturbance, however, has not yet been denied for its preference. Linear stability theory cannot give concrete prediction upon which mode will be preferred as the critical mode. Agreement between theoretical results and experimental ones is not satisfactory although the effect of the non-par-

allelism of the basic flow has recently been taken into account in the analysis by Hall and Morris [28]. This is due to the fact that neither an appropriate controlled disturbance nor sensitive detection of the onset of instability has been introduced in the experiments.

In the present experiment, release position of hot thermal plumes from the hot surface moves towards the edge of the hot surface with increase in Rayleigh number. This suggests that a hot thermal plume will be released when Rayleigh number based on the distance from the edge of the hot surface, $x = R - r$, exceeds a critical value. The value of x at the separation could be measured from flow visualization experiment. Critical Rayleigh number Ra_x based on x at the release position is plotted against Pr in Fig. 15. The value of Ra_x is a decreasing function of Pr. Results of other studies [27, 28], which measured the onset of longitudinal roll on a heated rectangular plate in air, are also shown in the figure. The onset Ra_x of traveling wave shows lower value than the onset of longitudinal roll of other studies.

Referring to these examples, we cannot unfortunately conclude what is the driving mechanism of the observed periodic release of the hot thermal plumes. At any rate, what is observed in the experiment is axisymmetric traveling wave. Because of the rapid growth of the boundary layer (the basic field is with a strong converging flow), the wave evolves very rapidly and exhibits fully nonlinear feature after a couple of wavelengths. As the Rayleigh number increases, non-axisymmetry appears on the axisymmetric wave pattern in the center region on the bottom plate. There are two possible origins for the non-axisymmetric pattern. One is the buoyancy driven roll formation due to the pattern selection mechanism of the basic through flow. The other is a secondary instability mechanism of the secondary flow (primarily unstable axisymmetric mode). If the former is true, the traveling wave should bifurcate prior to the bifurcation of longitudinal roll. Therefore, there should be a local region in which the axisymmetric wave interacts with the radial roll. This is however most unlikely. No significant deformation on traveling waves is expected by an interaction between traveling waves which already developed to the fully nonlinear disturbance and the radial roll which is still in linear or weakly nonlinear stage with sufficiently small amplitude. With further increase in the Rayleigh number, the onset location of non-axisymmetric pattern moves to larger r. For sufficiently large value of Ra, $Ra = 4 \times 10^7$ for example, we can observe radial roll pattern locally in the center region on the bottom surface. Prior to an onset of turbulence, breaking of axisymmetry thus occurs.

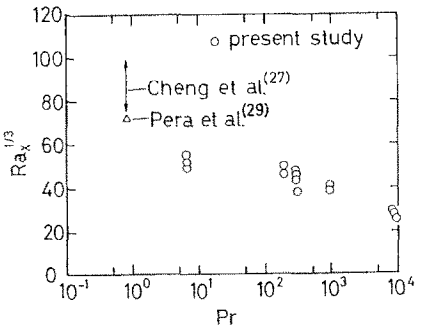

FIG. 15. Plot of critical Rayleigh number against Prandtl number.

The experimental results indicate that integrated quantity, such as average heat transfer rate on a hemispherical surface, is not sensitive to transition from laminar to turbulent and the effects of the transition appear after it is completed. In the present study, heat transfer mechanisms along hemispherical surface from $Ra \sim \times 10^5$, where hot thermal plumes began to release periodically, till $Ra \sim 10^9$, where flow became fully turbulent, are laminar mechanisms as far as the average Nu is concerned.

6. CONCLUSIONS

The following conclusions are obtained from the present study.

Correlation between average Nusselt number and Rayleigh number obtained from the experiment are expressed by equations (2) and (3)

Flow patterns in a hemisphere were classified into four flow regimes, i.e. steady circulating flow regime for $Ra < 2 \times 10^5$, flow regime of periodic hot thermal plume for $2 \times 10^5 \leqslant Ra \leqslant 4 \times 10^7$, flow regime of irregular hot thermal plume for $4 \times 10^7 < Ra < 10^9$ and turbulent flow regime for $Ra > 10^9$. Wavy structure of the plumes in flow direction indicates hot thermal plumes should be understood as traveling waves. They are axisymmetric for $Ra \leqslant 2 \times 10^6$. For $Ra > 10^6$, a thermal boundary layer is formed near the hot and cold surfaces and the average fluid temperature becomes uniform except in the vicinity of both surfaces. Large circulating flow exists in the hemisphere below $Ra < 10^9$, which rises at the center of the hot surface and descends along the hemispherical surface. This circulating flow almost vanishes at about $Ra \sim 10^9$ and finally the flow becomes turbulent with irregular thermal plumes.

Hot thermal plumes released from the hot surface reach the top of the hemisphere for $Ra \leqslant 5 \times 10^8$, however, they are dissipated just above the hot surface and cannot reach the top surface for $Ra \geqslant 5 \times 10^8$. Experimental results show that transition from laminar to turbulent occurs at $Ra \sim 10^9$.

Numerical analysis showed similar thermal plumes to the ones observed in the flow visualization experiment. Relationship between Nusselt number and Rayleigh number obtained by the numerical analysis agreed well with the experimental results for low Rayleigh number.

REFERENCES

1. D. Dropkin and E. F. C. Somerscales, Heat transfer by natural convection in liquids confined by two parallel

plates which are inclined at various angles with respect to the horizontal, *Trans. ASME. Ser. C* **87,** 77–84 (1965).
2. T. Y. Chu and R. J. Goldstein, Turbulent convection in a horizontal layer of water, *J. Fluid Mech.* **60,** 141–159 (1973).
3. D. E. Fitzjarrald, An experimental study of turbulent convection of air, *J. Fluid Mech.* **73,** 693–719 (1976).
4. H. Tanaka and H. Miyata, Turbulent natural convection in a horizontal water layer heated from below, *Int. J. Heat Mass Transfer* **23,** 1273–1281 (1980).
5. R. J. Goldstein, H. D. Chiang and D. L. See, High Rayleigh number convection in a horizontal enclosure, *J. Fluid Mech* **213,** 111–126 (1990).
6. R. K. MacGregor and A. F. Emery, Free convection through vertical plane layers—moderate and high Prandtl number fluids, *Trans. ASME. Ser. C* **91,** 391–403 (1969).
7. N. Seki, S. Fukusako and H. Inaba, Visual observation of natural convective flow in a narrow vertical cavity, *J. Fluid Mech.* **84,** 695–704 (1978).
8. N. Seki, S. Fukusako and S. Inaba, Heat transfer in an enclosed cavity with a relatively small aspect-ratio, *Bull. Fac. Eng., Hokkaido University* **87,** 1–10 (1978).
9. N. Seki, S. Fukusako and A. Yamaguchi, An experimental study of free convective heat transfer in a parallelogrammic enclosure, *Trans. ASME. Ser. C* **105,** 433–439 (1983).
10. M. S. Bohn, A. T. Kirkpatrick and D. A. Olson, Experimental study of three dimensional natural convection high-Rayleigh number, *Trans. ASME. Ser. C* **106,** 339–345 (1984).
11. S. Weinbaum, Natural convection in a horizontal circular cylinder, *J. Fluid Mech.* **18,** 409–437 (1964).
12. E. H. Bishop, L. R. Mack and J. A. Scanlon, Heat transfer by natural convection between concentric spheres, *Int. J. Heat Mass Transfer* **9,** 649–662 (1966).
13. B. Farouk and S. I. Güçeri, Laminar and turbulent natural convection in the annulus between horizontal concentric cylinders, *Trans. ASME. Ser. C* **104,** 631–636 (1982).
14. D. M. Poulikakos and A. Bejan, The dynamics of an attic space, *J. Fluid Mech.* **131,** 251–269 (1983).
15. E. M. Campo, Analysis of laminar natural convection in a triangular enclosure, *Numer. Heat Transfer* **13,** 353–372 (1988).
16. S. W. Lam, R. Gani and J. G. Symons, Experimental and numerical studies of natural convection in trapezoidal cavities, *Trans. ASME. Ser. C* **111,** 372–377 (1989).
17. S. H. Davis, Convection in a box: linear theory, *J. Fluid Mech.* **30,** 465–478 (1967).
18. R. Krishnamurti, On the transition to turbulent convection. Part 1. The transition from two- to three-dimensional flow, *J. Fluid Mech.* **42,** 309–325 (1970).
19. K. T. Yang, Transitions and bifurcations in laminar buoyant flow in confined enclosures, *Trans. ASME. Ser. C* **110,** 1191–1204 (1988).
20. S. M. ElSherbiny, G. D. Raithby and K. G. T. Hollands, Heat transfer by natural convection across vertical and inclined air layers, *Trans. ASME. Ser. C* **104,** 96–102 (1982).
21. Y. Lee and A. K. Seppo, Multicellular natural convection in a vertical slot, *J. Fluid Mech.* **126,** 91–121 (1983).
22. Y. Shiina, Heat transfer from the inner surface of a sphere by free convection, *Heat Transfer—Jap. Res.* **18,** 70–86 (1989).
23. R. B. Husar and E. M. Sparrow, Patterns of free convection flow adjacent to horizontal heated surfaces, *Int. J. Heat Mass Transfer* **11,** 1206–1208 (1968).
24. S. V. Patankar, *Numerical Heat Transfer and Fluid Flow.* Hemisphere, New York (1980).
25. R. J. Goldstein and K. S. Lau, Laminar natural convection from a horizontal plate and the influence of plate-edge extensions, *J. Fluid Mech.* **129,** 55–75 (1983).
26. K. C. Cheng and Y. W. Kim, Flow visualization studies on vortex instability of natural convection flow over horizontal and slightly inclined constant temperature plates, *Trans. ASME. Ser. C* **110,** 608–615 (1988).
27. L. Pera and B. Gebhart, On the stability of natural convection boundary layer flow over horizontal and slightly inclines surfaces, *Int. J. Heat Mass Transfer* **16,** 1147–1162 (1973).
28. P. Hall and H. Morris, On the instability of boundary layers on heated flat plates, *J. Fluid Mech.* **245,** 367–400 (1992).
29. R. E. Kelly, The onset and development of Rayleigh–Bénard convection in shear flows: a review. In *Physicochemical Hydrodynamics* (Edited by D. B. Spalding), pp. 65–79. Advance Publications, London (1977).
30. *Handbook of Chemical Engineering* (in Japanese). Maruzen (1978).
31. *Thermodynamic Properties* 1 ~ 10 (in Japanese). Maruzen (1963–1972).
32. Shinetsu Silicone Technical data T6-7C, T6-8B (in Japanese), Shinetsu Chemistry Co. Ltd.